Learning Robust Model Predictive Control for Voltage Control of Islanded Microgrid

Sahand Kiani, Ali Salmanpour, Mohsen Hamzeh, *Member, IEEE*, and Hamed Kebriaei, *Senior Member, IEEE*

***Abstract*— This paper proposes a novel control design for voltage tracking of an islanded AC microgrid in the presence of nonlinear loads and parametric uncertainties at the primary level of control. The proposed method is based on the Tube-Based Robust Model Predictive Control (RMPC), an online optimization-based method which can handle the constraints and uncertainties as well. The challenge with this method is the conservativeness imposed by designing the tube based on the worst-case scenario of the uncertainties. This weakness is amended in this paper by employing a combination of a learning-based Gaussian Process (GP) regression and Tube-Based RMPC. The advantage of using GP is that both the mean and variance of the loads are predicted at each iteration based on the real data, and the resulted values of mean and the bound of confidence are utilized to design the tube in Tube-Based RMPC. The theoretical results are also provided to prove the recursive feasibility and stability of the proposed learning based Tube-Based RMPC. Finally, the simulation results are carried out on both single and multiple DG (Distributed Generation) units.**

***Note to Practitioners*—In this paper, we present a new way to control the voltage in an islanded microgrid to improve Power Quality (PQ). The method we propose is based on an online optimization technique called Tube-Based Robust Model Predictive Control. It can handle uncertainties and disturbances that occur when the microgrid operates independently, ensuring the voltage remains stable. However, there's a challenge with this method. It tends to be too cautious because it assumes the worst-case scenario for uncertainties. To make the control more efficient, we improve it by combining a learning-based technique called Gaussian Process regression with Tube-Based RMPC. The advantage of using GP is that it predicts the uncertainty of the electrical devices based on real data. We use these predictions to design the control in Tube-Based RMPC more accurately. We also provide theoretical results to show that our new learning-based control is reliable and stable. We tested our approach through computer simulations on different scenarios with one or multiple power sources in the microgrid. The results show the effectiveness of our control design in regulating the voltage even with uncertain and nonlinear loads. Overall, this paper suggests a practical and reliable way to control the voltage in an independent microgrid using a combination of online optimization and learning techniques.**

***Index Terms*— Gaussian process regression, islanded microgrid, robust model predictive control, voltage control.**

Manuscript received 22 January 2024; revised 6 March 2024; accepted 3 April 2024. This article was recommended for publication by Editor Q. Zhao upon evaluation of the reviewers' comments. The work of Hamed Kebriaei was supported in part by the Institute for Research in Fundamental Sciences (IPM) under Grant CS 1402-4-208. *(Corresponding author: Hamed Kebriaei.)*

Sahand Kiani is with the School of Electrical and Computer Engineering, Pennsylvania State University, State College, PA 16802 USA (e-mail: sahand.kiani1374@gmail.com).

Ali Salmanpour and Mohsen Hamzeh are with the School of Electrical and Computer Engineering, College of Engineering, University of Tehran, Tehran 1417935840, Iran (e-mail: a.salmanpour9@gmail.com; mohsenhamzeh@ut.ac.ir).

Hamed Kebriaei is with the School of Electrical and Computer Engineering, College of Engineering, University of Tehran, Tehran 1417935840, Iran, and also with the School of Computer Science, Institute for Research in Fundamental Sciences (IPM), Tehran 1953833511, Iran (e-mail: kebriaei@ut.ac.ir).

Color versions of one or more figures in this article are available at https://doi.org/10.1109/TASE.2024.3388018.

Digital Object Identifier 10.1109/TASE.2024.3388018

I. Introduction

SEVERAL reasons make the microgrids work in an islanded mode, such as faults in the main grid, high prices of grid's power, and supplying remote areas [1]. Improving local reliability, power quality, providing lower investment costs, and reducing emissions are microgrids' main features [2]. Voltage regulation is a vital requirement to maintain the power delivery stable and consistent in an islanded microgrid. Proper voltage regulation ensures reliable and efficient operation of the microgrid, especially in remote and isolated areas where grid connections are not available [3].

Traditional voltage regulation methods, such as PI control, fuzzy logic control, sliding mode control, and adaptive control have been widely used in microgrids [4], [5]. PI control is a simple and reliable method that provides good stability, but it has limited performance when dealing with nonlinear and uncertain systems [6]. Fuzzy logic control is a more flexible method that can handle nonlinear and uncertain systems but requires more complex modeling and control design [7]. In recent years, researchers have focused on developing advanced control strategies, such as MPC, to improve the performance and stability of islanded microgrids [8]. MPC is an optimization-based control method that can handle both linear and nonlinear systems with constraints, making it more suitable for complex and uncertain systems. It has been shown that in terms of steady-state performance, MPC outperforms sliding mode control [9]. Explicit prediction of future plant behavior and the computational efficiency of MPC using current systems measurements made this online method favorable in microgrids. In [10], the authors conducted simulations and experimental tests to compare the performance of the proposed MPC method with traditional control methods such as PI control and fuzzy logic control. The results showed that the MPC-based control method outperformed traditional methods in terms of voltage regulation performance, especially under conditions of varying loads and disturbances.

To face with the uncertainties and disturbances existing in the model, Tube-Based RMPC is proposed [11]. The feedback

law tights the real state trajectories inside a bound centered around the nominal system trajectories. However, this method can be conservative since the control law is obtained based on the worst-case scenario of uncertainties [12].

To mitigate conservativeness in Tube-Based RMPC, various regression methods have been proposed to improve the accuracy of the tube approximation [13]. One such method is Gaussian Process Regression (GPR). GPR is a supervised learning-based method that has shown promise in estimating and compensating for disturbances in MPC while reducing conservativeness and improving computational efficiency [14]. GPR estimates a bound of confidence of prediction, in addition to the mean value, which is directly used in robust controller design [15]. By using GPR to estimate disturbances in real time, the performance of Tube-Based RMPC is enhanced by reducing the need for conservative control strategies.

In this paper, we propose Learning Tube-Based RMPC (LRMPC) method that utilizes GPR to estimate the current of the load as the disturbance, while also considering the upper bound of parametric uncertainties in the robust controller design. To the best of the authors' knowledge, neither Tube-Based RMPC nor LRMPC has been used to control the voltage of an islanded microgrid at the primary level. The adoption of the proposed method, Learning Robust MPC, is driven by the lack of our knowledge about the real bound of uncertainties and disturbances within the system. In the absence of concrete information about these bounds, the default approach is to plan for the worst-case values of disturbances/uncertainties, leading to a conservative strategy. However, this conservative approach may not accurately reflect the actual, often lower, levels of these bounds. The Learning Robust MPC is designed to overcome this limitation by offering a more precise and potentially less restrictive estimation of these bounds, enhancing the effectiveness of the control mechanism [16], [17]. Our latest findings indicate that when the actual bounds of disturbances/uncertainties deviate significantly from these worst-case estimates, the performance of the Learning Robust MPC shows a marked improvement over the traditional Robust MPC. This advancement stems from our limited knowledge about the precise limits of uncertainties and disturbances, which can now be more accurately estimated using real data. In scenarios where such data is unavailable, we resort to assuming the worst-case values, a method that tends to be overly cautious. The greater the disparity between the actual and the worst-case values of disturbances, the more pronounced the efficiency of the Learning Robust MPC becomes in comparison to the conventional Robust MPC.

The proposed method is initially developed for a single-DG islanded microgrid, where nonlinear loads and parametric uncertainties can significantly affect the system's performance and power quality. Nevertheless, we also demonstrate its effectiveness for multiple DGs as well. The main contributions of this paper are:

- Using Tube-Based RMPC to enhance the performance of voltage regulation of an islanded microgrid in the presence of parametric uncertainties and disturbances (including harmonic loads) to meet PQ standards
- Using Gaussian Process as a learning method to calculate the tubes online with less conservativeness and estimate the loads to be used in shaping the control law
- Proposing recursive feasibility and stability analysis for the system, in which the effect of GP is considered
- Demonstrating the effectiveness of the proposed control method at the primary level while multiple DGs exist in an islanded microgrid

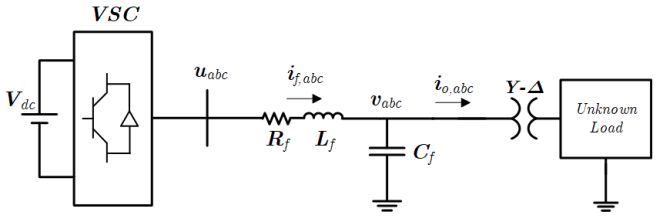

Fig. 1. Single-DG unit connected to an unknown load.

Notation: The Euclidean norm of x vector is denoted by $\|x\|$. Respectively, The term $x^T Qx$ denotes $\|x\|_Q^2$. The Pontryagin difference of sets $A \subseteq \mathbb{R}^n$ and $B \subseteq \mathbb{R}^n$ is denoted by $A \ominus B = \{a | a + b \in A, \forall b \in B\}$, and the Minkowski sum is $A \oplus B = \{a + b | a \in A, b \in B\}$. We define the addition of set and vector as $x \oplus B = \{x + b | x \in \mathbb{R}^n, b \in B\}$. The set multiplication is defined as if $M \in R^{m \times n}$ then $MA := \{Ma | a \in A\}$. I_n is used to show the identity matrix of size n. The pseudo-inverse of a $m \times n$ matrix X when $n \leq m$ is $A^\dagger = (A^T A)^{-1} A^T$. The set $\psi \subseteq \mathbb{R}^n$ is positive invariant if and only if no solution starting inside ψ can leave ψ. i.e. $\forall x(0) \in \psi$, $\varphi(k, x(0)) \in \psi \ \forall k > 0$, for dynamical system $x(k+1) = f(x(k))$ with $\varphi(k, x(0))$ as its solution.

II. Model of an Islanded Microgrid

A single-DG in an islanded microgrid is considered [18], [19]. Overhauls, faults, high energy prices, and supplying remote areas are among the reasons to switch a microgrid from the grid-connected mode to the islanded mode. Various disturbances might arise when the microgrid is in islanded mode, such as current of loads. The parametric uncertainties in the inverter's LC filter are another source of disturbance. This paper takes into account the effect of parametric uncertainties and loads as disturbances to the microgrid and proposes an appropriate control method to compensate for such effects. The microgrid is defined by three main components in islanded mode: DG, converter, and loads.

As shown in Fig. 1, by neglecting the nonlinear dynamics of the DC-Bus and using Kirchhoff's voltage and current laws, the dynamical model can be derived as follows

$$\begin{cases} i_{f,abc} = i_{o,abc} + C_f \dfrac{dv_{abc}}{dt} \\ u_{abc} = L_f \dfrac{di_{f,abc}}{dt} + R_f i_{f,abc} + v_{abc} \end{cases} \tag{1}$$

where $i_{f,abc}$ and $i_{o,abc}$ stand for three-phase inductor current and inverter output current. respectively, u_{abc} and v_{abc} show the inverter output voltage before LC filter and output terminal voltage. Moreover, R_f, L_f, and C_f are the parameters of the

filter. To exploit the advantages of the d-q frame for smoother analysis, Park transformation is used as follows

$$\begin{bmatrix} \dot{V}_d \\ \dot{V}_q \\ \dot{I}_{fd} \\ \dot{I}_{fq} \end{bmatrix} = \begin{bmatrix} \omega_0 V_q + \frac{1}{C_f} I_{fd} - \frac{1}{C_f} I_{od} \\ -\omega_0 V_d + \frac{1}{C_f} I_{fq} - \frac{1}{C_f} I_{oq} \\ -\frac{1}{L_f} V_d - \frac{R_f}{L_f} I_{fd} + \omega_0 I_{fq} + \frac{1}{L_f} V_{od} \\ -\frac{1}{L_f} V_q - \omega_0 I_{fd} - \frac{R_f}{L_f} I_{fq} + \frac{1}{L_f} V_{oq} \end{bmatrix} \quad (2)$$

Equation (2) forms the small-signal dynamical model of a single-DG unit in d-q frame. This equation governs the dynamic response of the system to ensure stability under rapid changes and disturbances, and it is pivotal for the robust operation of the microgrid at the most immediate level. To make the model compatible with MPC, the model is discretized as follows

$$x(k+1) = Ax(k) + Bu(k) + \underbrace{Eu_d(k)}_{w_1(k)} + \underbrace{\Delta Ax(k) + \Delta Bu(k)}_{w_2(x,u,k)}$$
$$y = Cx(k), \quad (3)$$

where $x = [V_d \ V_q \ I_{fd} \ I_{fq}]^T \in X \subseteq R^4$ denotes the state vector and $u = [V_{od} \ V_{oq}]^T \in U \subseteq R^2, u_d = [I_{od} \ I_{oq}]$ are control and disturbance input, respectively, and $y = [V_d \ V_q] \in R^2$ is the output vector. The vectors $w_1(k)$ and $w_2(x,u,k)$ represent the effect of the current of the loads and parametric uncertainties in the 3-phase lines, respectively. During the operation of an inverter, the capacitance, the inductance, and the resistance of the LC filter vary as time passes. These changes are bounded, unpredictable, and adversely affect voltage tracking. This effect is captured by the uncertainty matrices ΔA and ΔB, obtained by substituting $C_f + \Delta C_f$ for C_f, $L_f + \Delta L_f$ for L_f, and $R_f + \Delta R_f$ for R_f in (2), respectively. The matrices will be defined as

$$A = \begin{bmatrix} 0 & \omega_0 & \frac{1}{C_f} & 0 \\ -\omega_0 & 0 & 0 & \frac{1}{C_f} \\ -\frac{1}{L_f} & 0 & -\frac{R_f}{L_f} & \omega_0 \\ 0 & -\frac{1}{L_f} & -\omega_0 & -\frac{R_f}{L_f} \end{bmatrix}, B = \begin{bmatrix} 0 & 0 \\ 0 & 0 \\ \frac{1}{L_f} & 0 \\ 0 & \frac{1}{L_f} \end{bmatrix}$$
$$E = \begin{bmatrix} -\frac{1}{C_f} & 0 \\ 0 & -\frac{1}{C_f} \\ 0 & 0 \\ 0 & 0 \end{bmatrix}, C = \begin{bmatrix} 1 & 0 & 0 & 0 \\ 0 & 1 & 0 & 0 \end{bmatrix}$$

Although our method is proposed on the primary level of control, we aim to show that it is able to work while we have multiple DGs [20]. To do so, the power sharing loop is responsible for managing power among multiple DGs using Droop method as follows:

$$f_i = f_{n_i} - m_i P_{DG_i},$$
$$v_{d_i}^* = V_{n_i} - n_i Q_{DG_i},$$
$$v_{q_i}^* = 0, \quad (4)$$

where m_{P_i} and n_{Q_i} are the frequency and voltage droop gains, respectively. V_{n_i} and f_{n_i} are the desired frequency and voltage for i-th DG unit, respectively. This is where the traditional droop control comes into play, aligning with the established practices in microgrids.

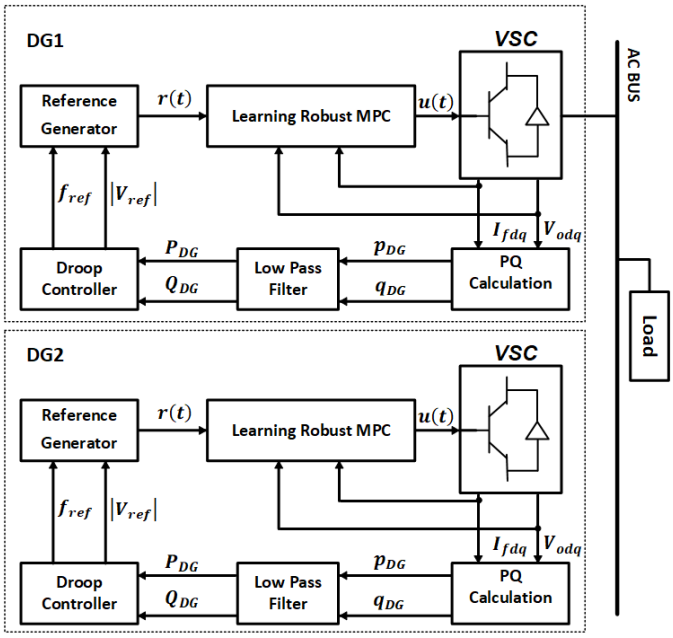

Fig. 2. Hierarchical framework of the proposed control method.

By delineating the control strategy across these two levels, our system leverages the fast-acting, robust control provided by the Learning Robust MPC, while ensuring that its capability to handle the steady-state regulation and power sharing tasks among multiple DGs. This dual-level strategy is validated by our simulation results. The figure below illustrates the hierarchical framework

where V_{odq} and I_{fdq} represent the voltage and current at the load terminal in the d-q frame, respectively. p_{DG} and q_{DG} denote the instantaneous active and reactive power. The Low Pass Filter (LPF) generates the filtered powers, which are then utilized in the droop unit to generate the reference values. As we are using the droop control method, we meticulously monitor frequency to effectively balance power sharing among DGs. This process involves careful consideration of active power distribution and voltage regulation for reactive power management. While our secondary level control does not address frequency and voltage restorations when they deviate, as these are beyond the scope of this paper, the variation in frequency changes then apply to the primary level of control. In the primary control level, we take an integral from the deviated frequency to provide the angle and apply this angle to Park Transformation. Our proposed method remains responsive to these frequency shifts.

This paper follows a novel approach to facing uncertainties and disturbances stated in (3). $w_1(k)$, known as the current of the load, is the measured disturbance. GP estimator is utilized to learn the mean and the variance of $w_1(k)$. On the other hand, the upper bound for the parametric uncertainty $w_2(x,u,k)$ is predetermined and known, i.e. $\|w_2(x,u,k)\|_\infty \leq L_2$. It should be noted that the pattern of parametric uncertainties related to the LC filter depends on the materials used in the inductor and capacitance, electric flux, and temperature. As a result, in order to estimate these values, the data should be gathered in laboratory circumstances or from the designer. Therefore, we only use a worst-case bound for parametric uncertainty

$w_2(x,u,k)$. The estimated mean and variance of $w_1(k)$ and the bound of $w_2(x,u,k)$ will be used to design Tube-Based RMPC. In what follows, we introduce the GP estimator of load $w_1(k)$ and Tube-Based RMPC as two main components of the proposed scheme.

III. Preliminary Results

A. Load's Current Prediction Using Gaussian Process

Loads are considered the most regular disturbances in islanded microgrids. GP uses the measured output current of the inverter as a time series for predicting the load current in an islanded microgrid. Here, GPR is employed as one of the most useful Bayesian nonparametric models. By using GPR, not only an estimate from the load current is attained, but also we can estimate a confidence interval which will be used as a bound in designing Tube-Based RMPC. Since we estimate this bound using real data, it would be less conservative compared to the worst-case bound.

Consider the standard linear regression model with Gaussian noise

$$\tilde{w}_1(k_i) = w_1(k_i) + \varepsilon(k_i) \tag{5}$$

where $\widetilde{\omega}_1(k_i)$ denotes measured value, $\varepsilon(k_i)$ represents an additive noise. $\omega_1(k_i)$ is the disturbance of the DG at time instant k_i. The noise $\varepsilon \sim N(0,\delta_\varepsilon^2)$ has the property of independent and identically distributed (i.i.d) Gaussian distribution with zero mean and variance δ_ε^2. We introduce $\widetilde{\mathbf{w}}_1(\tau) = [\widetilde{\omega}_1(k_1), \widetilde{\omega}_1(k_2), \ldots, \widetilde{\omega}_1(k_n)]$ as measured value vector, $\tau = [k_1, k_2, \ldots, k_n]$ as the sample time vector and $\mathbf{w}_1(\tau) = [\omega_1(k_1), \omega_1(k_2), \ldots, \omega_1(k_n)]$ as load disturbance vector. The aim is to assign a distribution over $\mathbf{w}_1(\tau)$ given the measured values of $\widetilde{\mathbf{w}}_1(\tau)$ using GP [21]. The distribution function of the measured vector is considered to be drawn from a multivariate Gaussian distribution as follows [22]

$$p(\tilde{\mathbf{w}}_1(\tau)) = \mathcal{N}(\mu(\tau), C(\tau,\tau)) \tag{6}$$

where $\mu(\tau) = [m(k_1), \ldots, m(k_n)]$ is denoted as the vector of mean functions $m(\tau) = \mathbb{E}[\tilde{w}(\tau)]$. $C(\tau,\tau)$ defined as follows

$$C(\tau,\tau) = \begin{pmatrix} c(k_1,k_1) & c(k_1,k_2) & \ldots & c(k_1,k_n) \\ c(k_2,k_1) & c(k_2,k_2) & \ldots & c(k_2,k_n) \\ \vdots & \vdots & \vdots & \vdots \\ c(k_n,k_1) & c(k_n,k_2) & \ldots & c(k_n,k_n) \end{pmatrix} \tag{7}$$

is known as the covariance matrix whose elements are covariance kernel functions between two training inputs. As it has been discussed in [22], choosing the kernel function depends on the knowledge of data. In this paper, the Radial Basis Function (RBF) is used as the kernel function $c(k_i,k_j) = h^2 exp[-(\frac{k_i-k_j}{\lambda})^2]$ in the covariance matrix of GP. RBF has two hyperparameters. The length scale λ determines the length of the wiggle in the function, and the output scale h determines the average distance of the function away from the mean. The training data encompasses a series of these current measurements taken evenly spaced with a regular sampling rate, denoted as k_1 to k_n. This series forms the basis for calculating matrices such as $C(\tau,\tau)$ and $(C(\tau,\tau)+\sigma I)^{-1}$, where τ represent the array of time instances $[k_1, \cdots, k_n]$. The process of updating these calculations is repeated each time new current data is measured. Hyperparameter selection is facilitated by the K-fold cross-validation technique. Initially, the dataset is partitioned into K-subsets of nearly equal size, known as K-folds. For each fold, the model undergoes training with a distinct combination of hyperparameters, after which the prediction error is calculated. Ultimately, the set of hyperparameters that results in the lowest prediction error is chosen [23]. The algorithm for K-Fold cross validation is proposed in [24], [25].

RBF assumes that points close to each other in the 2-norm sense are more correlated. The input of the GP is the measured current of the load that is sampled from a time-series signal. The length scale hyperparameter within this kernel plays a key role in determining how this correlation diminishes with increasing time difference.

To generate a prediction using GPR, we need to compute the posterior distribution function of $\mathbf{w_1}$ and then predict unseen data by calculating the predictive posterior [26]. The posterior function consists of two components; likelihood function and prior distribution. The likelihood function is defined as follows

$$p(\tilde{\mathbf{w}}_1(\tau)|\mathbf{w}_1(\tau)) \sim \mathcal{N}(\tilde{\mathbf{w}}_1(\tau)|\mathbf{w}_1(\tau), \sigma_N^2 I) \tag{8}$$

where the mean of the function is centered on an arbitrary $\mathbf{w}_1$. The second component is the prior defined as follows

$$p(\mathbf{w}_1(\tau)|\tau) \sim \mathcal{N}(\mathbf{w}_1(\tau)|\mathbf{0}, C(\tau,\tau)) \tag{9}$$

It is assumed the mean of the prior is always a zero vector. Nevertheless, as we see in what follows, GP is able to model a general mean function from the kernel-based covariance function. From (8) and (9), the posterior over function is achieved by the likelihood function times the prior over function

$$p(\mathbf{w}_1(\tau)|\tau, \tilde{\mathbf{w}}_1(\tau)) \propto p(\tilde{\mathbf{w}}_1(\tau)|\mathbf{w}_1(\tau)) p(\mathbf{w}_1(\tau)|\tau) \tag{10}$$

Both the likelihood and the prior are Gaussian. As a result, posterior over function will have a Gaussian distribution as follows

$$\begin{aligned} p(\mathbf{w}_1(\tau)|\tau, \tilde{\mathbf{w}}_1(\tau)) &\sim \mathcal{N}(\mathbf{w}_1(\tau)|\bar{\mu}, \bar{\Sigma}) \\ \bar{\mu} &= C(\tau,\tau)[C(\tau,\tau)+\sigma_N^2 I]^{-1}\tilde{\mathbf{w}}_1(\tau) \\ \bar{\Sigma} &= C(\tau,\tau)[C(\tau,\tau)+\sigma_N^2 I]^{-1}\sigma_N^2 I \end{aligned} \tag{11}$$

Once the posterior over function is obtained, The predictive posterior can be computed as follows, which is used to predict the mean and variance of unseen data.

$$\begin{aligned} &p(\tilde{\mathbf{w}}_1^*(\tau)|\tau_*, \tau, \tilde{\mathbf{w}}_1(\tau)) \\ &= \int p(\tilde{\mathbf{w}}_1^*(\tau)|\tau_*, \mathbf{w}_1(\tau), \tau) p(\mathbf{w}_1(\tau)|\tau, \tilde{\mathbf{w}}_1(\tau)) \mathrm{d}\mathbf{w}_1(\tau) \end{aligned} \tag{12}$$

where $\tilde{\mathbf{w}}_1^*(\tau)$ denotes to a vector of new unseen measured values with the new sample time matrix τ_*. The term in the integral, the posterior over function, is computed in (11). The training data set is obtained from the measured value of the output current of the inverter, which is equal to the load's current while there is a single-DG, at k_1 to k_n. The likelihood of new unseen data $\tilde{w}_1(k_{n+1})$ can be calculated, and it is a Gaussian distribution as well.

Initially, when there is limited data, the model might exhibit higher prediction errors due to insufficient information to accurately capture the system's dynamics. As mentioned in [27] (Theorem 11), under two assumptions which are: the observations are perturbed by zero-mean, i.i.d. Gaussian noise, and sampling the unknown function with Gaussian distribution, we can assure that the model improves with new data. It is acknowledged in the literature that modeling load distributions as Gaussian is standard practice, as evidenced by studies such as [28], [29] [30]. However, it is important to recognize that in practical scenarios, the actual distribution of the load may not be Gaussian. In such instances, GP offers an optimal approximation by fitting the best possible Gaussian distribution to the observed data. In practical scenarios, if newly acquired data does not result in a non-increasing variance, we exclude that specific sample from our analysis to maintain adherence to our assumptions. Additionally, the current of the load has a cyclic pattern, suggesting that collected data that is used for updating GP are informative enough when GP faces new data. It is worth mentioning that by collecting enough data, the learning error will uniformly converge to zero almost surely.

B. Tube-Based Robust Model Predictive Control

By neglecting the disturbances and uncertainties of the real system in (3), the nominal system will be defined as follows

$$\tilde{x}(k+1) = A\tilde{x}(k) + B\tilde{u}(k); \quad \tilde{x}(0) = \tilde{x}_0, \tag{13}$$

where $\tilde{x}(k) \in \bar{X}$ and $\tilde{u}(k) \in \bar{U}$ are the nominal trajectory and the nominal input, respectively. The sets $\bar{X}$ and $\bar{U}$ will be defined in a way so that the robust performance is achieved. The MPC controller works in this way: At each MPC shot t, $t \in \{0,\ 1, \ldots,\ T-N+1\}$, the control law is computed for the period $[t, t+1, \ldots, t+N-1]$ by solving an optimization problem. Nevertheless, only the first element of the computed input sequence is applied to the system, and the state of the system evolves for one step accordingly. This process continues for the next shots until the control inputs for the whole control horizon are computed. The control and prediction horizon of MPC are considered to be T and N, respectively. In our problem, the objective is to ensure that the voltage of the load terminal is tracked in the reference signal. The reference signal is a setpoint while a single-DG unit is available in the islanded microgrid. However, by considering multiple DG units, the reference signal varies as time passes. The optimal nominal trajectories can be obtained by solving the following:

$$\min_{\tilde{x}_{0|0}, \tilde{u}_t} \sum_{k=0}^{N-1} \|\tilde{x}_{k|t} - r(t)\|_Q + \|\tilde{u}_{k|t} - u_r\|_R + \|\tilde{x}_{N|t} - r(t)\|_P \tag{14a}$$

$$\text{s.t.} \quad \tilde{x}_{k+1|t} = A\tilde{x}_{k|t} + B\tilde{u}_{k|t}, \tag{14b}$$

$$\tilde{x}_{k|t} \in \bar{X}, \tilde{u}_{k|t} \in \bar{U}, \tag{14c}$$

$$(\tilde{x}_{N|t} - r(t)) \in \tilde{X}_f \subseteq \bar{X}, \tag{14d}$$

$$(\tilde{x}_{0|t} - x_t) \in S_K(\infty), \tag{14e}$$

where $r(t)$ is piecewise constant reference. Following the methodologies in [31] and [32], we chose to use a linear programming approach MPC due to its simplicity and faster solution times compared to an equivalently sized quadratic programming model. $\tilde{x}_{k|t}$ and $\tilde{u}_{k|t}$ are known as the predicted state and control input of the t^{th} MPC shot, which give k step ahead prediction of the state and input starting from time-step t, and $\tilde{u}_t = [\tilde{u}_{0|t}, \ldots, \tilde{u}_{N-1|t}]$. u_r is the control input that adjusts the nominal system (13) equilibrium point to match the reference signal $r(t)$. The matrices Q and R are semi-positive definite and positive definite. The terminal weighting matrix P, is a positive definite matrix. $\tilde{X}_f$ represents the terminal set and is designed to ensure the stability condition [33]. The set $S_K(\infty)$ will guarantee to keep the error bounded. The calculation method of $S_K(\infty)$ is discussed at the end of this section. Practically, YALMIP Toolbox is utilized [34] to solve this problem, which uses Linear Programming (LP) solver. By solving the MPC problem in (14), the optimal nominal input and the corresponding optimal state trajectory will be found as follows

$$\begin{aligned}
\tilde{u}^* &= (\tilde{u}^*(0), \ldots, \tilde{u}^*(T-1)) \\
&= [\tilde{u}^*_{0|0}, \ldots, \tilde{u}^*_{T-N|T-N}, \tilde{u}^*_{T-N+1|T-N}, \ldots, \tilde{u}^*_{T-1|T-N}] \\
\tilde{x}^* &= (\tilde{x}^*(0), \ldots, \tilde{x}^*(T-1), \tilde{x}^*(T)) \\
&= [\tilde{x}^*_{0|0}, \ldots, \tilde{x}^*_{T-N+1|T-N}, \ldots, \tilde{x}^*_{T-1|T-N}, \tilde{x}^*_{T|T-N}].
\end{aligned} \tag{15}$$

Clearly, the real trajectory of the system, x, will be different from the nominal trajectory, $\tilde{x}$, due to the presence of uncertainties and disturbances. The real control input of the system, u, is designed in a way that the real trajectory of the system lies as close to the nominal trajectory as possible, using the following feedback policy

$$u(k) = \tilde{u}^*(k) + K(x(k) - \tilde{x}^*(k)), \tag{16}$$

where the feedback gain $K \in R^{2\times 4}$ is obtained by LQR technique to make the matrix $\tilde{A} = A + BK$ Schur stable under the controllability of the pair (A,B). In (16), the gain K compensates deviations from nominal trajectories. By calculating the difference between the real system and nominal system and substituting the feedback policy (16) in (3) the error dynamic becomes

$$e(k+1) = \tilde{A}e(k) + w(x, u, k), \tag{17}$$

where $e := x - \tilde{x}^*$ and $w(x, u, k) = w_1(k) + w_2(x, u, k)$ whose set is denoted by W. As it was mentioned and also will be discussed in the next subsection in more detail, this set is estimated at each iteration using the GP estimator of $w_1(k)$ and the worst-case bound on $w_2(x, u, k)$.

The accumulative set of disturbances, $S_K(k)$, is defined as

$$S_K(k) := \sum_{j=0}^{k-1} \tilde{A}^j W = W \oplus \tilde{A}W \oplus \cdots \oplus \tilde{A}^{k-1}W, \tag{18}$$

As shown in [33], by setting $x(0) = \tilde{x}(0) = x_0$, since $\tilde{A}$ is Schur, $S_K(\infty)$ exists and is positive invariant for the error dynamics in (17). The feedback policy (16) assures that the state of the real system (3) is compelled to be close to that of the nominal system (13).

As $x = \tilde{x}^* + e$, and knowing that K is constant, the state of the nominal trajectories will be the center of the tube generated by feedback policy (16) is defined as follows

$$Z(k) := \tilde{x}^*(k) \oplus S_K(\infty) \tag{19}$$

Finally, to maintain the state and control input in X and U, the state and control input set of the nominal system need to be defined as follows

$$\bar{U} \triangleq U \ominus K S_K(\infty), \bar{X} \triangleq X \ominus S_K(\infty), \tilde{X}_f \subset X \ominus S_K(\infty), \tag{20}$$

Proposition 1: Considering $x(k) \in Z(k)$ and $u(k) = \tilde{u}^*(k) + K(x(k) - \tilde{x}^*(k))$, then $x(k+1) \in Z(k+1)$ for all $w(x,u,k) \in W$ [35].

As a result, the solution of (3) using control policy (16) as its input lies in the tube $Z(k)$ for every admissible disturbance sequence [33].

IV. Learning Tube-Based Robust MPC for Islanded Microgrid

In this subsection, we show how the set W and accordingly $S_K(\infty)$ can be estimated using GP and the available bound on w_2. This estimation will then be used for tube shaping and formulating the MPC controller of the real system.

Since the disturbance vector $w_1(k)$ is measured directly, it will be used to collect the training data. We get the sample-time vector of training data as $[k_1, k_2, \cdots, k_n] = [0, \ldots, k-1]$ and the prediction sample-time as $k_{n+1} = k$. Therefore, by estimating $\mu_*(k)$ and $\sigma_*^2(k)$ using (11), the distribution of $w_1(k)$ is obtained as GP $\sim \mathcal{N}(\mu_*(k), \sigma_*^2(k))$. Given $\Delta\mu_t = \mu_*(t+1) - \mu_*(t)$, and under the assumption that $\|\Delta\mu_t\|_2 \leq \epsilon$ has a constant bound, we can define the set $\hat{W}$ accordingly, where set $\hat{W}$ serves as an estimation of the set W:

$$\begin{aligned} \hat{W}(k) = \{ & w(x,u,k) \in R^n : \\ & \|\hat{w}_1(k) - \mu_*(k)\|_{\sigma_*^{-1}(k)} \leq \chi_n^2(\vartheta) + \epsilon, \\ & \|w_2(x,u,k)\|_\infty \leq L_2\}, \end{aligned} \tag{21}$$

where χ_n^2 and ϑ denote the chi-distribution with n degree of freedom and the confidence interval. More details are discussed in [36]. By substituting $\hat{W}(k)$ into (18), the set $\hat{S}_K(\infty)$ can be defined as follows

$$\hat{S}_K(k) := \sum_{j=0}^{k-1} \tilde{A}^j \hat{W} = \hat{W} \oplus \tilde{A}\hat{W} \oplus \cdots \oplus \tilde{A}^{k-1}\hat{W}, \tag{22}$$

Accordingly, the new state and control input set of the nominal system will be

$$\hat{U} \triangleq U \ominus K \hat{S}_K(\infty), \hat{X} \triangleq X \ominus \hat{S}_K(\infty), \hat{X}_f \subset X \ominus \hat{S}_K(\infty), \tag{23}$$

In this way, we can replace constraint (14e) and (14c) in optimization problem (14) with $(\tilde{x}_{N|t} - r(t)) \in \hat{X}_f \subseteq \hat{X}$ and $\tilde{x}_{k|t} \in \hat{X}, \tilde{u}_{k|t} \in \hat{U}$, Then LRMPC optimization problem can be defined as follows:

$$\min_{\hat{x}_{0|0}, \hat{u}_t} \sum_{k=0}^{N-1} \|\hat{x}_{k|t} - r(t)\|_Q + \|\hat{u}_{k|t} - u_r\|_R + \|\hat{x}_{N|t} - r(t)\|_P \tag{24a}$$

Algorithm 1 Learning Tube-Based Robust Model Predictive Control

Input: Initial Dataset, Initial time $t = t_0$
Output: Control input u_t at each time step
while *True* **do**
  Measure current state x_t;
  Update GP's Dataset and compute μ_* and σ_*;
  Update tube and constraint using (21), (22), (23);
  Set $x_{0|t} = x_t$, and solve optimization problem (24);
  Set control input $\tilde{u}_t = \tilde{u}_{0|t}$;
  Implement control action $u_t = \tilde{u}_t + K(x_t - \tilde{x}_{0|t})$;
  Increment time $t = t + 1$ and repeat from step 1;
end

$$\hat{x}_{k+1|t} = A\hat{x}_{k|t} + B\hat{u}_{k|t} + \mu_*(t), \tag{24b}$$
$$\tilde{x}_{k+1|t} = A\tilde{x}_{k|t} + B\tilde{u}_{k|t}, \tag{24c}$$
$$\hat{u}_{k|t} = \tilde{u}_{k|t} + K(\hat{x}_{k|t} - \tilde{x}_{k|t}), \tag{24d}$$
$$\tilde{x}_{k|t} \in \hat{X}, \tilde{u}_{k|t} \in \hat{U}, \tag{24e}$$
$$\hat{x}_{0|t} = \hat{x}_{1|t-1}, \tag{24f}$$
$$(\tilde{x}_{0|t} - x_t) \in \hat{S}_K(\infty), \tag{24g}$$
$$(\tilde{x}_{N|t} - r(t)) \in \hat{X}_f \subseteq \hat{X}, \tag{24h}$$

where $\hat{x}_t$ is the estimated state and $\hat{X}_f$ is the invariant terminal set which is computed using the disturbance set introduced in (21) and the method presented in [37]. The procedure of designing LRMPC is illustrated in Algorithm 1.

V. Analytical Results

A. Recursive Feasibility

An MPC is called recursively feasible if it always keeps the states in a region from where the online optimization problem has a feasible solution [38]. In other words, if the problem (24) has a feasible solution for the initial condition x_0 and it remains feasible for any subsequent states x_i of the controlled system (3), then the MPC problem is recursively feasible [39].

Lemma 1: Let's define $u_r = B^\dagger(r - Ar)$. Then by having $\tilde{u}_{N|t} = K(\tilde{x}_{N|t} - r) + u_r$, an invariant terminal set $\hat{X}_f$ exists such that if $\tilde{x}_{N|t} - r \in \hat{X}_f$ then $A\tilde{x}_{N|t} + B\tilde{u}_{N|t} - r \in \hat{X}_f$.

Proof: proof is provided in [37].

Now we can express the Recursive Feasibility theorem.

Theorem 1: . Assume that $\hat{X}_f$ is a terminal invariant set given in Lemma 1. If the MPC problem has a feasible solution for the initial condition x_0, then the solution of MPC is feasible for all the times.

Proof: The proof is based on mathematical induction. For this purpose, it is assumed that the optimization problem (24) at time t has a solution like $([\tilde{x}^*_{0|t}, \tilde{x}^*_{1|t}, \cdots, \tilde{x}^*_{N|t}], [\tilde{u}^*_{0|t}, \tilde{u}^*_{1|t}, \cdots, \tilde{u}^*_{N-1|t}])$.

According to Eq. (21), the estimated set $\hat{W}(k)$ depends on $\sigma_*^{-1}(k)$. Since $\sigma_*(k)$ is non-increasing [27], $\sigma_*^{-1}(k)$ is non-decreasing and hence we have $\hat{W}(k+1) \subseteq \hat{W}(k)$. It can be concluded that $Z(k+1) \subseteq Z(k)$ which shows that our feasible set is larger or equal compared to the previous time instant.

The tube $Z(k)$ is an invariant set for the error dynamics (17), therefore, $([\tilde{x}^*_{1|t}, \tilde{x}^*_{2|t}, \tilde{x}^*_{3|t}, \cdots, \tilde{x}^*_{N|t}],\ [\tilde{u}^*_{1|t}, \tilde{u}^*_{2|t}, \cdots, \tilde{u}^*_{N-1|t}])$ is feasible solution for MPC problem at $t+1$ from 1 to $N-1$ prediction horizon. Also, according to the constraint $(\tilde{x}_{N|t} - r) \in \hat{X}_f$ and Lemma 1, we can say that there is an input $\tilde{u}$ and final state $\tilde{x}_{N|t+1}$ that satisfies the equation (24h). Hence, a feasible solution for optimization (24) at time $t+1$ can be suggested as follows

$$\begin{aligned}(\boldsymbol{x}_{t+1}, \boldsymbol{u}_{t+1}) = ([&\tilde{x}^*_{1|t}, \tilde{x}^*_{2|t}, \cdots, \tilde{x}^*_{N|t},\\ &A\tilde{x}_{N|t} + B(K(\tilde{x}_{N|t} - r) + u_r)],\\ &[\tilde{u}^*_{0|t}, \tilde{u}^*_{1|t}, \cdots, \tilde{u}^*_{N-1|t}, K(\tilde{x}_{N|t} - r) + u_r])\end{aligned} \tag{25}$$

Therefore, recursive feasibility is established.

B. Stability

It is also important to verify the stability of the system under the proposed LRMPC algorithm. The following theorem expresses the stability of the system.

Theorem 2: Using control policy (16) with the nominal input derived from the optimization problem (14) subject to the system (3), the following properties are satisfied:

1) $x(k) \in X$, $u(k) \in U$ for all $k \geq 0$.
2) The closed-loop system is Input-to-State-Stable (ISS).

Proof. Let $\hat{e}_{k|t} = \hat{x}_{k-1|t+1} - \hat{x}_{k|t}$. Then, for $k = 1, \ldots, N-1$, we have:

$$\begin{aligned}\hat{x}_{k|t+1} &= A\hat{x}_{k-1|t+1} + B\hat{x}_{k|t+1} + \mu_*(t+1)\\ &= A(\hat{x}_{k|t} + \hat{e}_{k|t}) + BK(\hat{x}_{k|t} + \hat{e}_{k|t} - \tilde{x}_{k|t})\\ &\quad + B\tilde{u}_{k|t} + \mu_*(t) + \Delta\mu_t\\ &= \hat{x}_{k+1|t} + \tilde{A}\hat{e}_{k|t} + \Delta\mu_t\\ &\Rightarrow \hat{e}_{k+1|t} = \tilde{A}\hat{e}_{k|t} + \Delta\mu_t\end{aligned} \tag{26}$$

since $\hat{x}_{0|t+1} = \hat{x}_{1|t}$, it follows that $\hat{e}_{0|t} = 0$. Therefore, utilizing (26), we obtain:

$$\hat{e}_{k|t} = \tilde{A}^k\hat{e}_{0|t} + \sum_{i=0}^{k-1}\left(\tilde{A}^i\Delta\mu_t\right) = \sum_{i=0}^{k-1}\left(\tilde{A}^i\right)\Delta\mu_t \tag{27}$$

additionally, we will have:

$$\left\|\sum_{i=0}^{N}\tilde{A}^i\Delta\mu_t\right\| \leq \sum_{i=0}^{\infty}\left(\bar{\sigma}_{\tilde{A}}\right)^i\epsilon = \frac{\epsilon}{1-\bar{\sigma}_{\tilde{A}}}, \tag{28}$$

where $\bar{\sigma}_{\tilde{A}}$ denotes the maximum singular values of $\tilde{A}$. Utilizing (27) and (28), we deduce the error bound as follows:

$$\left\|\hat{e}_{k|t}\right\| \leq \frac{\epsilon}{1-\bar{\sigma}_{\tilde{A}}} \tag{29}$$

Further, for $k = N$ we derive the following equation:

$$\begin{aligned}&\hat{x}_{N|t+1} - r\\ &= \tilde{A}(\hat{x}_{N|t} - r) + \sum_{i=0}^{N}\tilde{A}^i\Delta\mu_t + \mu_*(t+1) + Ar + Bu_r - r\\ &= \tilde{A}(\hat{x}_{N|t} - r) + \sum_{i=0}^{N}\tilde{A}^i\Delta\mu_t + \mu_*(t+1).\end{aligned} \tag{30}$$

In the following, by using the Lyapunov method, the stability of the system will be expressed. $J(t)$ is defined as the cost function used in the LRMPC controller as follows:

$$J(t) = \sum_{k=0}^{N-1}\|\hat{x}_{k|t} - r\|_Q + \|\hat{u}_{k|t} - u_r\|_R + \|\hat{x}_{N|t} - r\|_P \tag{31}$$

then, the Lyapunov function can be defined as the optimal cost function obtained from (24) as follows

$$v_t = J_*(t) \tag{32}$$

v_t is clearly positive. According to the Lyapunov theorem, if the Lyapunov function can be proved to be decreasing over the time, then the system is stable.

$$v_{t+1} - v_t = J_*(t+1) - J_*(t) \leq \hat{J}(t+1) - J_*(t) \tag{33}$$

where $J_*(t+1)$ represents the optimal cost at time $t+1$, and $\hat{J}(t+1)$ is the cost function obtained by substituting (25) into (31), the following equation is derived:

$$\begin{aligned}v_{t+1} - v_t \leq &-\left(\|\hat{x}_{0|t} - r\|_Q + \|\hat{u}_{0|t} - u_r\|_R\right)\\ &+ \sum_{k=0}^{N-1}\Big\{\|\hat{x}_{k|t+1} - r\|_Q - \|\hat{x}_{k+1|t} - r\|_Q\\ &+\|\hat{u}_{k|t+1} - u_r\|_R - \|\hat{u}_{k+1|t} - u_r\|_R\Big\}\\ &+ \|\hat{x}_{N|t+1} - r\|_P - \|\hat{x}_{N|t} - r\|_P.\end{aligned} \tag{34}$$

Assume $Q = \hat{Q}\hat{Q}^T$, $P = \hat{P}\hat{P}^T$, and $R = \hat{R}\hat{R}^T$ are symmetric matrices, and $\hat{Q}$, $\hat{R}$, and $\hat{P}$ are Cholesky decompositions of Q, R, and P, respectively. Using (29), we obtain:

$$\begin{aligned}v_{t+1} - v_t \leq &-\left(\|\hat{x}_{0|t} - r\|_Q + \|\hat{u}_{0|t} - u_r\|_R\right) + \sum_{k=0}^{N-1}\frac{\bar{\sigma}_{\tilde{Q}}\epsilon}{1-\bar{\sigma}_{\tilde{A}}}\\ &+ \|\hat{Q}^T(\hat{x}_{N|t} - r)\| - \|\hat{P}^T(\hat{x}_{N|t} - r)\|\\ &+ \|\hat{R}^T(\hat{u}_{N|t} - u_r)\| + \|\hat{P}^T(\hat{x}_{N|t+1} - r)\|.\end{aligned} \tag{35}$$

where $\bar{\sigma}_{\tilde{Q}} = \bar{\sigma}_{\hat{Q}} + \bar{\sigma}_{\hat{R}K}$, while $\bar{\sigma}_{\hat{Q}}$ and $\bar{\sigma}_{\hat{R}K}$ denote the maximum singular values of $\hat{Q}$ and $\hat{R}K$, respectively. By utilize (30), Equation (35) simplifies to the following form:

$$\begin{aligned}v_{t+1} - v_t &\leq \|\hat{Q}^T\left(\hat{x}_{N|t} - r\right)\| + \|\hat{R}^T\left(\hat{u}_{N|t} - u_r\right)\|\\ &\quad + \|\hat{P}^T\left(\hat{x}_{N|t+1} - r\right)\| - \|\hat{P}^T\left(\hat{x}_{N|t} - r\right)\|\\ &\quad - \left(\|\hat{x}_{0|t} - r\|_Q + \|\hat{u}_{0|t} - u_r\|_R\right)\\ &\quad + \frac{(N-1)\bar{\sigma}_{\tilde{Q}}}{1-\bar{\sigma}_{\tilde{A}}}\epsilon + \|\mu_*(t+1)\|\\ &\leq \|\hat{Q}^T\left(\hat{x}_{N|t} - r\right)\| + \|\hat{R}^TK(\hat{x}_{N|t} - r)\|\\ &\quad + \|\hat{P}^TA_K(\hat{x}_{N|t} - r)\| - \left(\|\hat{P}^T\left(\hat{x}_{N|t} - r\right)\|\right)\\ &\quad - \left(\|\hat{x}_{0|t} - r\|_Q + \|\hat{u}_{0|t} - u_r\|_R\right) + \rho\epsilon\\ &\quad + \|\mu_*(t+1)\|\end{aligned} \tag{36}$$

where $\rho = \frac{\left((N-1)\bar{\sigma}_{\tilde{Q}} + \bar{\sigma}_{\hat{P}}\right)}{1-\bar{\sigma}_{\tilde{A}}}$, and $\bar{\sigma}_{\hat{P}}$ denotes the maximum singular value of $\hat{P}$. Following the framework of theorem (2)

TABLE I
PARAMETERS OF DG

Parameter	Value	Remark
R_f	1.5 mΩ	Converter and LC Filter
L_f	100 mH	
C_f	100 μF	
f_0	60 Hz	
S_{base}	3 MVA	
V_{base}	600 V	
V_{dc}	2000 V	
Transformer ratio (Y/Δ)	600/13800 V	
T_s	250 μs	MPC
Z_{Line1}, Z_{Line2}	0.35+j1.16 Ω	Droop Parameters
n_1,n_2	0.5, 0.87 V/MVAr	
m_1,m_2	0.6, 0.9 Hz/MW	

from [31], we introduce matrices H and $\tilde{P}$ satisfying:

$$\tilde{P}A_K - H\tilde{P} = 0, \quad \|H\| \leq 1, \tag{37}$$

From the above equation, $\hat{P}$ can be derived as follows

$$\hat{P} = \frac{\left(\|\hat{Q}\tilde{P}^{\dagger}\| + \|K\hat{R}\tilde{P}^{\dagger}\|\right)}{1 - \|H\|}\tilde{P} \tag{38}$$

where $\tilde{P}^{\dagger}$ being the pseudoinverse of $\tilde{P}$. From proposition (1) in [31]:

$$\|\hat{Q}^T(\hat{x}_{N|t} - r)\| + \|\hat{R}^T K(\hat{x}_{N|t} - r)\| + \|\hat{P}^T A_K(\hat{x}_{N|t} - r)\| - (\|\hat{P}^T(\hat{x}_{N|t} - r)\|) \leq 0, \tag{39}$$

Consequently, the Equation (36) simplifies to:

$$v_{t+1} - v_t \leq -(\|\hat{x}_{0|t} - r\|_Q + \|\hat{u}_{0|t} - u_r\|_R) + \rho\epsilon + \|\mu_*(t+1)\|. \tag{40}$$

Therefore, the estimated region of convergence of the system (3) is $\{\hat{x} \mid \|\hat{x} - r\|_Q \leq \rho\epsilon + \|\mu_*(t+1)\|\}$. Here, $\rho\epsilon$ represents the term indicating how load deviation affects the region of convergence, while $\|\mu_*(t+1)\|$ represents how the estimated upper bound affects the region of attraction.

VI. Simulation Results

To evaluate the performance of the proposed LRMPC, first, a single-DG microgrid shown in Fig. 1 is simulated to show the efficiency of voltage control. Then, two DGs are connected in parallel, and power sharing is done using droop control. The microgrid parameters are listed in Table I.

In our case studies, we compare "Tube-Based RMPC", "MPC", and the conventional PI controller against "Learning Tube-Based RMPC" under identical operational conditions. "LRMPC" is then applied to a power-sharing loop in a microgrid with multiple DGs. Simulations account for parametric uncertainties ($\Delta R_f = 0.1R_f$, $\Delta C_f = 0.1C_f$, $\Delta L_f = 0.2L_f$) and use THD, low steady-state error, and dynamic response as evaluation criteria. Factors like parasitic elements, as well as sampling and computational delays, are also considered. THD permissible range is defined by the IEEE standard [40] (i.e., 5%). The simulations utilized Matlab,

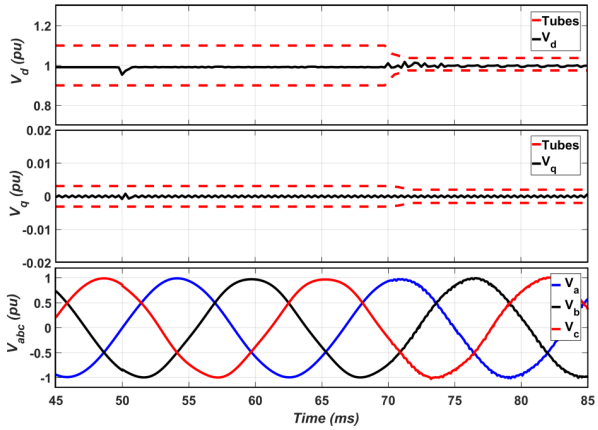

Fig. 3. Voltage regulation using Learning Tube-Based RMPC: voltages in d-q frame and abc-frame while the constant impedance and harmonic loads are connected at t=50ms and t = 70ms.

Python, YALMIP, and the SimPowerSystems toolbox, with the Scikit-Learn toolbox specifically employed for implementing GP and K-Fold Cross Validation techniques [23].

The proposed method assesses worst-case variations by setting bounds for disturbances and uncertainties that shape the tubes, calculated online for precise analysis. It includes a 10ms initial warm-up phase for GP training. The warm-up phase, a crucial initial step, minimizes estimation errors before collecting ample data. The GP training uses load current data batch over 35ms to build the covariance matrix. RBF hyperparameters $h = 1.37$, $\lambda = 0.02$ are optimized offline via K-Fold Cross Validation, with each fold comprising a vector of load current samples. Each vector has a dimension of $\mathbf{R}^{140\times1}$, reflecting 140 samples per fold. This results from sampling a continuous signal over 35ms intervals at a rate of 250μs.

GP estimation of new data before each control horizon takes 62μs, well below the sampling time of 250μs, allowing for regular GP updates with new data at every control horizon. Shaping the control policy mentioned in (16) will be a crucial step in Tube-Based RMPC. It can be proven that, under the controllability of (A,B) and observability of (A,$\sqrt{Q}$), the gain K obtained from above LQR ensures the optimality and stability of the system [41]. Using the LQR technique, matrix K is obtained as follows

$$K = \begin{bmatrix} -2.79\times10^{-4} & -1.14\times10^{-4} & 0.0369 & 0.018 \\ -0.0028 & 0.0057 & 0.018 & 0.1141 \end{bmatrix}, \tag{41}$$

If K is incorrect, the controller may fail to accurately track voltage, risking system instability. Considering noisy observations with variance $\delta_\epsilon^2 = 0.01$, a 95% confidence interval shapes the tubes as a bound. The method is implementable with a Technosoft SA MBE.300.E500 PMSM. With an 85ms prediction horizon and a 1.25ms control horizon, LRMPC averages 0.027455s to execute.

A. Harmonic Loads

This section evaluates the proposed method against MPC, Tube-Based RMPC, and PI. The test scenario involves connecting a 340kVA constant impedance load (PF=0.9) to an islanded microgrid at 50ms and adding a nonlinear load with

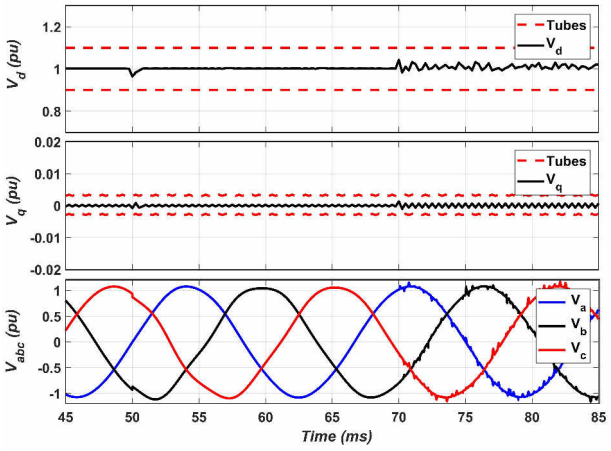

Fig. 4. Voltage regulation using Tube-Based RMPC: voltages in d-q frame and abc-frame while the constant impedance and harmonic loads are connected at t=50ms and t=70ms.

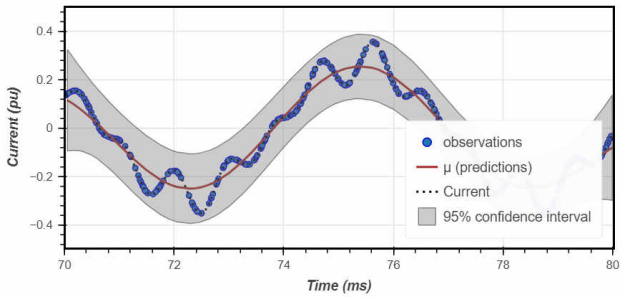

Fig. 5. Gaussian process regression is used to predict the harmonic current and shape a 95% confidence interval with noisy observations.

5th and 7th harmonics at 70ms. The nonlinear load's current THD is around 38%.

Fig. 3 shows voltage drops upon connecting constant impedance, followed by GP estimations. The optimization uses these estimates for effective voltage regulation via LRMPC, achieving a voltage THD of 1.5%. Tubes tighten with more data at t = 70ms, enhancing learning efficiency.

Fig. 4 shows Tube-Based RMPC controlling voltage with larger tubes due to worst-case uncertainty assumptions, making it more conservative than LRMPC. This conservativeness is indicated by the tube widths in both Figs. 3 and 4. Without GP, Tube-Based RMPC experiences an increased voltage THD of 2.04%, highlighting GP's role in reducing conservativeness by estimating load currents.

In Fig. 5, we enhance load current estimation within a 95% confidence interval using μ_* for estimation and σ_*^2 for bounds, alongside calculated parametric uncertainty bounds in tubes. Oscillation increases cause a rise in estimated variance. There's a balance between mean estimation accuracy and the number of noisy samples. We opt for fewer observations for computational efficiency.

Table II outlines voltage regulation in an islanded microgrid across different harmonic and nonlinear conditions, highlighting the effectiveness of LRMPC with favorable voltage THDs. It compares this approach to a PI controller managing 5^{th}, 7^{th}, and 11^{th} harmonic loads at a current THD of 38%.

TABLE II
COMPARISON AMONG METHODS FOR DIFFERENT HARMONIC LOADS

Harmonics	Current THDs %	Voltage THDs %		
		LRMPC	RMPC	MPC
5^{th}, 7^{th}, 11^{th}	30.83	1.49	2.02	3.58
	41.69	1.52	2.07	3.67
	51.39	1.56	2.15	3.91
5^{th}, 11^{th}, 13^{th}	31.49	1.50	2.11	3.62
	44.62	1.58	2.24	3.76
	52.71	1.61	2.36	4.02

TABLE III
COMPARISON AMONG METHODS BASED ON VOLTAGE THDS - HARMONIC LOADS

LRMPC	Tube-Based RMPC	MPC	Conventional PI
1.50%	2.04%	3.62%	3.74%

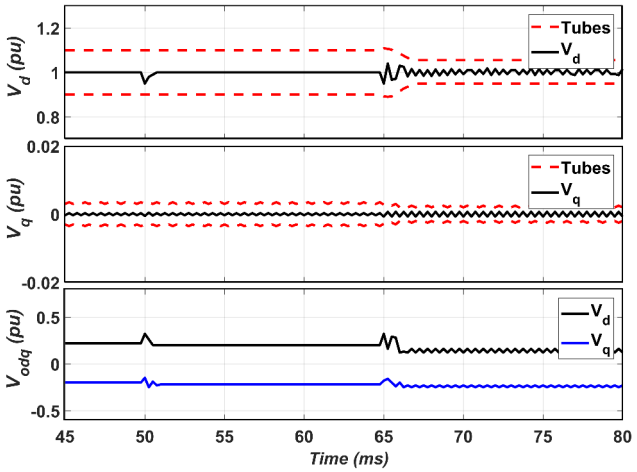

Fig. 6. Voltage regulation using Learning Tube-Based RMPC: learning results and control input in d-q frame and abc-frame while the constant impedance and harmonic loads are connected at t = 50 ms and t = 65 ms.

The conventional PI controller exhibits inferior performance relative to other methods, a discrepancy that intensifies as loads with higher harmonics are connected to the DG.

In Fig. 6, we have considered a constant impedance load beside the harmonic loads with 5^{th}, 11^{th}, and 13^{th} and the current THD of 44.62%. We showed how our control inputs change when the loads are connected to the single-DG.

B. Constant Power Loads

In this section, a 340kVA constant impedance load with PF = 0.9 is connected to the islanded microgrid at t = 50ms, and a 500kVA constant power load with PF = 1 parallel with a harmonic load consisting of 5^{th} and 7^{th} harmonics will be connected to the output terminal at t = 70ms. LRMPC is deployed for voltage regulation under these conditions, followed by a comparison with Tube-Based RMPC, MPC, and PI controller.

In Fig 7, LRMPC regulates the voltage with desirable voltage THD of 1.97%. Constant power load control, particularly in the context of microgrids, is a critical aspect of

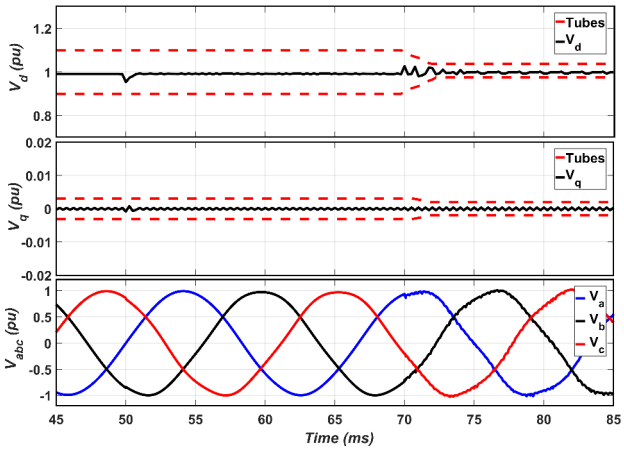

Fig. 7. Voltage regulation using Learning Tube-Based RMPC: voltages in d-q frame and abc-frame while the constant impedance and the constant power load parallel with harmonic load are connected at $t = 50$ ms and $t = 70$ ms.

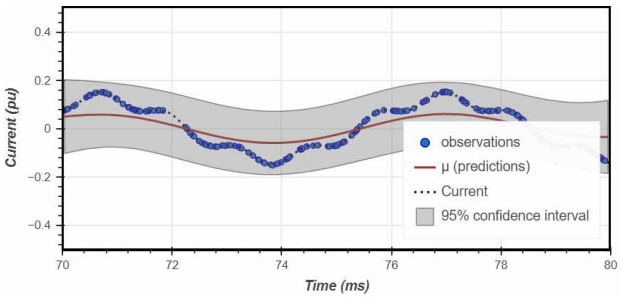

Fig. 8. Gaussian process regression is used to predict the current of the loads and shape a 95% confidence interval with noisy observations.

TABLE IV
COMPARISON AMONG METHODS BASED ON VOLTAGE THDS - CONSTANT POWER LOAD

LRMPC	Tube-Based RMPC	MPC	Conventional PI
1.97%	2.48%	3.79%	3.95%

maintaining stability and efficient operation. Using LRMPC, we can handle nonlinear loads together while ensuring the stability and high performance of the system. A comparison has been made in the following table among different methods as follows

In Fig. 8, GP is used to predict the current of the loads with 95% confidence interval. The predicted current will be used in the optimization, and the variance has been used to shape the tube with less conservativeness.

C. Droop Control for Power Sharing

LRMPC is introduced for primary control in single-DG units and can extend to microgrids with multiple DGs. For power-sharing, two DGs operating in parallel employ the droop control method. The output terminal's instantaneous voltage and current calculate active and reactive power, respectively. These powers are filtered by a 10Hz low pass filter to eliminate ripples. The resulting average powers, P_{DG} and Q_{DG}, serve as inputs for the droop controller,

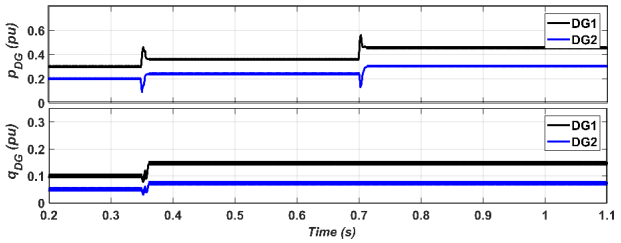

Fig. 9. Instantaneous power and reactive power of two DG units while a constant impedance and a constant power load are connected.

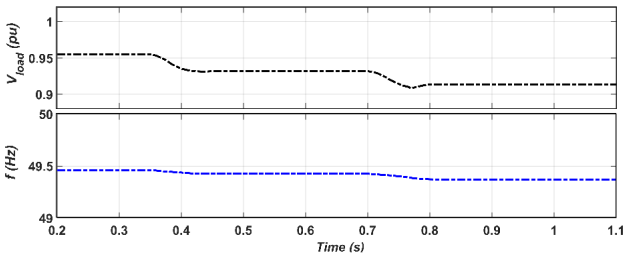

Fig. 10. Voltage and frequency of the load terminal.

generating reference signals according to Eq. (4). Droop control is crucial for parallel inverter operation, providing inherent synchronization and eliminating the need for a separate synchronization unit, effectively fulfilling the same role as a PLL [42].

Fig. 9 displays the active and reactive powers when a 340kVA (PF=0.9) and a 500kVA (PF=1) load are connected at 350ms and 700ms, respectively. The LPF (10Hz) smooths out ripples, ensuring power is shared among DG units according to droop characteristics. Despite noticeable power overshoots and undershoots due to load changes, these remain within acceptable limits, showcasing effective load change management.

Fig. 10 shows the voltage and frequency of the load terminal. The references from the droop controller will be used in LRMPC to force to track them. As the dynamics are slow, the performance of LRMPC is not affected significantly. The adaptive nature of the LRMPC allows for continuous improvement in tracking accuracy over time.

VII. CONCLUSION

This paper introduces a novel Learning Tube-Based RMPC for tracking AC inverter-based islanded microgrid voltage at the primary control level, effectively managing nonlinear loads and parametric uncertainties. GPR enhances Tube-Based RMPC design by reducing conservativeness, estimating loads, and shaping tubes online with available data. The proposed method's pros and cons are outlined below: (i): By using Tube-Based RMPC, the performance of voltage regulation of an islanded microgrid is enhanced in the presence of parametric uncertainties and load disturbances to meet PQ standards. (ii) The performance of Tube-Based RMPC is enhanced by incorporating a Gaussian Process method to estimate the mean value and the bound of uncertainties based on real data, which leads to less conservativeness compared to the worst-case design. (iii): Harmonic loads as a disturbance are handled

using Learning Tube-Based MPC. (iv): The computational cost of Learning Tube-Based MPC is increased compared to benchmarking methods like PI, MPC, and also Tube-Based MPCs. Our method, suitable for islanded microgrids with multiple DGs, utilizes droop control for power sharing. The recursive feasibility and stability of LRMPC are analytically confirmed. Comparisons with MPC, Tube-Based RMPC, and Learning Tube-Based RMPC in terms of THD, performance, and steady-state error demonstrate the proposed method's effectiveness.

REFERENCES

[1] N. M. Dehkordi, N. Sadati, and M. Hamzeh, "Fully distributed cooperative secondary frequency and voltage control of islanded microgrids," *IEEE Trans. Energy Convers.*, vol. 32, no. 2, pp. 675–685, Jun. 2017.

[2] M. H. Saeed, W. Fangzong, B. A. Kalwar, and S. Iqbal, "A review on microgrids' challenges & perspectives," *IEEE Access*, vol. 9, pp. 166502–166517, 2021.

[3] W. Huang, Z. Shuai, X. Shen, Y. Li, and Z. J. Shen, "Dynamical reconfigurable master–slave control architecture (DRMSCA) for voltage regulation in islanded microgrids," *IEEE Trans. Power Electron.*, vol. 37, no. 1, pp. 249–263, Jan. 2021.

[4] X. Shen, J. Liu, H. Lin, Y. Yin, A. M. Alcaide, and J. I. Leon, "Cascade control of grid-connected NPC converters via sliding mode technique," *IEEE Trans. Energy Convers.*, vol. 38, no. 3, pp. 1491–1500, Feb. 2023, doi: 10.1109/TEC.2023.3247432.

[5] V. Thomas, S. Kumaravel, and S. Ashok, "Fuzzy controller-based self-adaptive virtual synchronous machine for microgrid application," *IEEE Trans. Energy Convers.*, vol. 36, no. 3, pp. 2427–2437, Sep. 2021.

[6] N. R. Merritt, C. Chakraborty, and P. Bajpai, "New voltage control strategies for VSC-based DG units in an unbalanced microgrid," *IEEE Trans. Sustain. Energy*, vol. 8, no. 3, pp. 1127–1139, Jul. 2017.

[7] M. Huang, Y. Kang, and F. Liu, "A model predictive control strategy for voltage regulation in islanded microgrids," *IEEE Trans. Ind. Informat.*, vol. 14, no. 7, pp. 3013–3024, Jul. 2018.

[8] A. La Bella, S. R. Cominesi, C. Sandroni, and R. Scattolini, "Hierarchical predictive control of microgrids in islanded operation," *IEEE Trans. Autom. Sci. Eng.*, vol. 14, no. 2, pp. 536–546, Apr. 2017.

[9] G. P. Incremona, M. Cucuzzella, A. Ferrara, and L. Magni, "Model predictive control and sliding mode control for current sharing in microgrids," in *Proc. IEEE 56th Annu. Conf. Decis. Control (CDC)*. IEEE, Dec. 2017, pp. 2661–2666.

[10] P. Prabhakar and H. Vennila, "Comparison between PI, fuzzy & predictive techniques for statcom to improve the transient stability of microgrid," *IJMET*, vol. 8, no. 8, pp. 819–829, Aug. 2017, Art. no. IJMET_08_08_089.

[11] H. S. Abbas, G. Männel, C. H. né Hoffmann, and P. Rostalski, "Tube-based model predictive control for linear parameter-varying systems with bounded rate of parameter variation," *Automatica*, vol. 107, pp. 21–28, Sep. 2019, doi: 10.1016/j.automatica.2019.04.046.

[12] S. Mata, A. Zubizarreta, and C. Pinto, "Robust tube-based model predictive control for lateral path tracking," *IEEE Trans. Intell. Veh.*, vol. 4, no. 4, pp. 569–577, Dec. 2019.

[13] F. Li, H. Li, and Y. He, "Adaptive stochastic model predictive control of linear systems using Gaussian process regression," *IET Control Theory Appl.*, vol. 15, no. 5, pp. 683–693, Mar. 2021.

[14] L. Hewing, J. Kabzan, and M. N. Zeilinger, "Cautious model predictive control using Gaussian process regression," *IEEE Trans. Control Syst. Technol.*, vol. 28, no. 6, pp. 2736–2743, Nov. 2019, doi: 10.1109/TCST.2019.2949757.

[15] A. D. Bonzanini, J. A. Paulson, G. Makrygiorgos, and A. Mesbah, "Fast approximate learning-based multistage nonlinear model predictive control using Gaussian processes and deep neural networks," *Comput. Chem. Eng.*, vol. 145, Feb. 2021, Art. no. 107174.

[16] Y. Zheng, T. Zhang, S. Li, G. Zhang, and Y. Wang, "GP-based MPC with updating tube for safety control of unknown system," *Digit. Chem. Eng.*, vol. 4, Sep. 2022, Art. no. 100041.

[17] R. Soloperto, M. A. Müller, S. Trimpe, and F. Allgöwer, "Learning-based robust model predictive control with state-dependent uncertainty," *IFAC-PapersOnLine*, vol. 51, no. 20, pp. 442–447, 2018.

[18] D. De and V. Ramanarayanan, "Decentralized parallel operation of inverters sharing unbalanced and nonlinear loads," *IEEE Trans. Power Electron.*, vol. 25, no. 12, pp. 3015–3025, Dec. 2010.

[19] M. Babazadeh and H. Karimi, "A robust two-degree-of-freedom control strategy for an islanded microgrid," *IEEE Trans. Power Del.*, vol. 28, no. 3, pp. 1339–1347, Jul. 2013.

[20] M. K. Behera and L. C. Saikia, "An improved voltage and frequency control for islanded microgrid using BPF based droop control and optimal third harmonic injection PWM scheme," *IEEE Trans. Ind. Appl.*, vol. 58, no. 2, pp. 2483–2496, Mar. 2022.

[21] C. E. Rasmussen and C. K. I. Williams, *Gaussian Processes for Machine Learning*. (Adaptive computation and machine learning). Cambridge, MA, USA: MIT Press, 2006.

[22] S. Roberts, M. Osborne, M. Ebden, S. Reece, N. Gibson, and S. Aigrain, "Gaussian processes for time-series modelling," *Philos. Trans. Roy. Soc. London A, Math. Phys. Sci.*, vol. 371, no. 1984, p. 20110550, 2013.

[23] F. Pedregosa et al., "Scikit-learn: Machine learning in Python," *J. Mach. Learn. Res.*, vol. 12, pp. 2825–2830, Nov. 2011.

[24] Y. Jung, "Multiple predictingK-fold cross-validation for model selection," *J. Nonparametric Statist.*, vol. 30, no. 1, pp. 197–215, Jan. 2018.

[25] T. Fushiki, "Estimation of prediction error by using K-fold cross-validation," *Statist. Comput.*, vol. 21, no. 2, pp. 137–146, Apr. 2011.

[26] B. A. Swastanto, "Gaussian process regression for long-term time series forecasting," M.S. thesis, Delf Univ. Technol., Delf, The Netherlands, 2016. [Online]. Available: http://resolver.tudelft.nl/uuid:7f3916c9-795c-403f-bec8-5eb6caa3e398

[27] A. Lederer, J. Umlauft, and S. Hirche, "Uniform error and posterior variance bounds for Gaussian process regression with application to safe control," 2021, *arXiv:2101.05328*.

[28] Y. Yang, S. Li, W. Li, and M. Qu, "Power load probability density forecasting using Gaussian process quantile regression," *Appl. Energy*, vol. 213, pp. 499–509, Mar. 2018.

[29] T. Ma, D. A. Barajas-Solano, R. Huang, and A. M. Tartakovsky, "Electric load and power forecasting using ensemble Gaussian process regression," *J. Mach. Learn. Model. Comput.*, vol. 3, no. 2, pp. 87–110, 2022.

[30] A. Yadav, R. Bareth, M. Kochar, M. Pazoki, and R. A. E. Sehiemy, "Gaussian process regression-based load forecasting model," *IET Generat., Transmiss. Distrib.*, vol. 18, no. 5, pp. 899–910, Jul. 2023, doi: 10.1049/gtd2.12926.

[31] A. Bemporad, F. Borrelli, and M. Morari, "Model predictive control based on linear programming—The explicit solution," *IEEE Trans. Autom. Control*, vol. 47, no. 12, pp. 1974–1985, Dec. 2002.

[32] M. Leomanni, G. Bianchini, A. Garulli, A. Giannitrapani, and R. Quartullo, "Sum-of-norms model predictive control for spacecraft maneuvering," *IEEE Control Syst. Lett.*, vol. 3, no. 3, pp. 649–654, Jul. 2019.

[33] J. B. Rawlings, D. Q. Mayne, and M. Diehl, *Model Predictive Control: Theory, Computation, and Design*, vol. 2. Madison, WI, USA: Nob Hill Publishing, 2017.

[34] J. Lofberg, "YALMIP: A toolbox for modeling and optimization in MATLAB," in *Proc. IEEE Int. Conf. Robot. Autom.*, Sep. 2004, pp. 284–289.

[35] D. Q. Mayne, M. M. Seron, and S. V. Raković, "Robust model predictive control of constrained linear systems with bounded disturbances," *Automatica*, vol. 41, pp. 219–224, Feb. 2005.

[36] A. D. Bonzanini, D. B. Graves, and A. Mesbah, "Learning-based SMPC for reference tracking under state-dependent uncertainty: An application to atmospheric pressure plasma jets for plasma medicine," *IEEE Trans. Control Syst. Technol.*, vol. 30, no. 2, pp. 611–624, Mar. 2022.

[37] L. Fagiano and A. R. Teel, "Model predictive control with generalized terminal state constraint," *IFAC Proc. Volumes*, vol. 45, no. 17, pp. 299–304, 2012.

[38] L. Yang, A. Katnik, and N. Ozay, "Quickly finding recursively feasible solutions for MPC with discrete variables," in *Proc. IEEE Conf. Control Technol. Appl. (CCTA)*, Aug. 2019, pp. 374–381.

[39] J. Rawlings, D. Mayne, and M. Diehl, *Model Predictive Control: Theory, Computation, and Design*. CA, USA: Nob Hill Publishing, 2017.

[40] *IEEE Recommended Practice and Requirements for Harmonic Control in Electric Power Systems*, IEEE Standard 519-2014, 2014, pp. 1–29.

[41] D. P. Bertsekas, *Dynamic Programming and Optimal Control*, 3rd ed. Belmont, MA, USA: Athena Scientific, 2005.
[42] Q.-C. Zhong, "Synchronization mechanism of droop control," in *Power Electronics-Enabled Autonomous Power Systems: Next Generation Smart Grids*, 2020, pp. 227–243.

Sahand Kiani received the B.Sc. degree in electrical engineering from Arak University, Arak, Iran, in 2018, and the M.Sc. degree in control systems from the University of Tehran, Tehran, Iran, in 2023. He is currently pursuing the Ph.D. degree with The Pennsylvania State University, Pennsylvania, USA. His research focuses on optimization, reinforcement learning, and system identification.

Ali Salmanpour received the B.Sc. degree in electrical engineering and the M.Sc. degree in control systems engineering from the University of Tehran, Tehran, Iran, in 2015 and 2018, respectively, where he is currently pursuing the Ph.D. degree, focusing on learning model predictive control. His academic interests include MPC, learning control, and robust control.

Mohsen Hamzeh (Member, IEEE) received the B.Sc. and M.Sc. degrees in electrical engineering from the University of Tehran, Tehran, Iran, in 2006 and 2008, respectively, and the Ph.D. degree in electrical engineering from the Sharif University of Technology, Tehran, in 2012. From 2013 to 2018, he was an Assistant Professor with Shahid Beheshti University. In 2018, he joined the School of Electrical and Computer Engineering, University of Tehran. His research interests include photovoltaic systems, microgrid control, and the applications of power electronics in power distribution systems.

Hamed Kebriaei (Senior Member, IEEE) received the Ph.D. degree in control systems from the University of Tehran, Iran, in 2010. He is currently an Associate Professor of Control Systems with the School of Electrical and Computer Engineering, University of Tehran. His research interests include game theory, distributed optimization and multi agent reinforcement learning. He is a TC Member of IEEE-CSS in Networks and Communication Systems, and a Board Member of Control Systems Chapter, IEEE Iran Section. He received the Outstanding Reviewer Award from IEEE TRANSACTIONS ON CYBERNETICS in 2022 and the Outstanding Young Researcher Award from the University of Tehran in 2023. He has served as a Guest Editor for IEEE CONTROL SYSTEMS LETTERS in 2023.